

The Possible Mn Hyperfine Interactions and Oxidation States of the Manganese Cluster in OEC Using Multiline Signal (MLS) Simulation Data with Average of Weighted Computations

Bernard Baituti*

Botswana International University of Science and Technology, Private Bag 16, Palapye, Botswana

Abstract

Understanding the structure of oxygen evolving complex (OEC) fully still remains a challenge. Lately computational chemistry with the data from more detailed X-ray diffraction (XRD) OEC structure, has been used extensively in exploring the mechanisms of water oxidation in the OEC. The present study involves simulation studies of the X-band continuous wave electron-magnetic resonance (CW-EPR) generated S_2 state signals, to investigate whether the data is in agreement with the four manganese ions in the OEC, being organised as a '3+1' model or 'dimer of dimers' model. The question that still remains is how much does each Mn ion contribute to the "g²multiline" signal through its hyperfine interactions in OEC? This is revealed in part by the structure of multiline signal studied in this project. The method of data analysis involves numerical simulations of the experimental spectra on relevant models of the OEC cluster. The simulations of the X-band CW-EPR multiline spectra, revealed three manganese ions having hyperfine couplings with large anisotropy. These are most likely Mn^{III} centres and these clearly support the 'low' oxidation state OEC paradigm model, with a mean oxidation of 3.25 in the S_2 state. This is consistent with the earlier data, but the present results clearly indicate that heterogeneity in hyperfine couplings exist in samples as typically prepared.

Keywords: Computational; Oxidation; Spectra; Anisotropic

Abbreviations: CW-EPR: Continuous wave electron-paramagnetic resonance; ENDOR: Electron nuclear double resonance; EtOH: Ethanol; ML: Multiline; MLS: Multiline signal; NIR: Near Infrared; OEC: Oxygen-evolving complex; pPBQ: Phenyl-*p*-benzoquinone; PSII: Photosystem II; DDM: n-dodecyl- β -D-maltoside; XRD: X-ray diffraction.

Introduction

The 'multiline' signals are the hyperfine structured ⁵⁵Mn hyperfine EPR signals, from net spin 1/2 ground states, generated by trapping photosystem II (PSII) samples in the S_2 or S_0 intermediates at cryogenic temperature [1]. The S_2 multiline signal (MLS) exhibits approximately 20 resolved hyperfine peaks, with little g anisotropy, and the hyperfine interactions are readily measured in X-band CW-EPR due to them being large (couplings are of order 250 MHz or more). The intrinsic hyperfine tensors of Mn^{III} and Mn^{II}/Mn^{IV} are distinctive, when all ions are high spin, with Mn^{III} being highly anisotropic as a Jahn-Teller d⁴ ion, while Mn^{II}/Mn^{IV} are closer to isotropic (closed d sub-shell), being d⁵/d³ ions respectively. Therefore, based on this principle, determining the number of near isotropic versus anisotropic ⁵⁵Mn tensors seen in the S_2 state should be able to differentiate between the 'high' and 'low' oxidation state paradigms and define oxidation states of individual Mn centres. No Mn^I center should be present in this state [2]. But the 'multiline' signals observed have the 'spin projected' hyperfine interactions, due to the OEC being a sufficiently strongly exchanged coupled system (see below). Although the intrinsic 'single ion' hyperfine values are not seen, the fractional anisotropy of the hyperfine interactions will still be preserved, as the spin projection merely scales the overall tensor magnitude. Illumination of spinach PSII membrane samples, that were dissolved in approximately 3% ethanol (EtOH) buffer medium, is known to produce the most hyperfine structured broad form of the MLS [3]. Examples are shown in Figures 4 and 7. The spectrum exhibits approximately 17 resolved peaks, with one resonance obscured by the tyrosine radical signal near $g = 2.00$ having been subtracted using the WINEPR software. This results in

a gap within that region. This MLS bears a resemblance to that from anti-ferromagnetically coupled Mn^{III}-Mn^{IV} or Mn^{III}-Mn^{II} oxo-bridged dimers, though more lines are seen (signal ~180 mT wide) than typically seen in the model dimer compounds (16-peaks). In addition, a 'super-hyperfine' structure can be observed (~30 G spacing), especially in the upper field of the MLS [3]. The S_2 multiline signal is narrower than that from a known model tetramer (Mn^{III}, 3Mn^{IV}), which contains ~26 peaks and has a width of ~195 mT [4]. The strongly exchanged coupled centers of the OEC have net anti-ferromagnetic coupling in the S_2 state, with MLS arising from the $S_T = 1/2$ ground state, where total spin operator, $S_T = S_1 + S_2 + S_3 + S_4$ (S_{1-4} are the spins of the four manganese ions). Therefore the observed individual nuclear hyperfine couplings are given as $A_i = \rho_i \cdot A_{i(ion)}$ where ρ_i is the appropriate spin projection term for Mn centre i and these sum to unity for the total system. A typical sixteen-line pattern of an anti-ferromagnetically coupled dimer (Mn^{III}-Mn^{IV}) forms, with the projection coefficients of $\rho_{III} = 2$ and $\rho_{IV} = -1$, ($\rho_{III} + \rho_{IV} = 1$). Here A_{III} is $\sim 2 \cdot A_{IV}$, in isotropic value, while the Mn^{III} term is typically axial and highly anisotropic (Jahn-Teller d⁴ ion), while Mn^{IV} is nearly isotropic (d³ ion). From CW-EPR and electron nuclear double resonance (ENDOR) studies on the S_2 MLS generated in PS II core complexes, as also used in the present study, that one large anisotropic Mn hyperfine coupling, one intermediate (near isotropic) coupling and one smaller, anisotropic coupling are clearly resolved for the MLS [5]. The two larger couplings are broadly consistent with a

*Corresponding author: Bernard Baituti, Botswana International University of Science and Technology, Private Bag 16, Palapye, Botswana, Tel: +2674900117; Fax: +2674900102; E-mail: baitutib@biust.ac.bw

Received April 26, 2017; Accepted May 16, 2017; Published May 23, 2017

Citation: Baituti B (2017) The Possible Mn Hyperfine Interactions and Oxidation States of the Manganese Cluster in OEC Using Multiline Signal (MLS) Simulation Data with Average of Weighted Computations. J Phys Chem Biophys 7: 243. doi: 10.4172/2161-0398.1000243

Copyright: © 2017 Baituti B. This is an open-access article distributed under the terms of the Creative Commons Attribution License, which permits unrestricted use, distribution, and reproduction in any medium, provided the original author and source are credited.

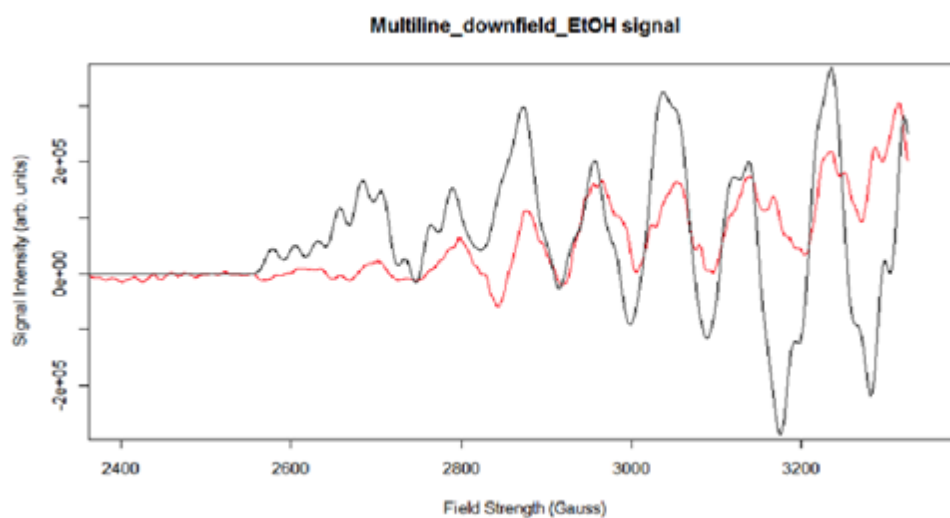


Figure 1a: The X-band CW-EPR difference down- field ML region. Experimental spectrum (red) and best-fit simulation (black). Spectrometer conditions: centre field 282.5 mT; frequency 9.634273 GHz; modulation amplitude 9.6 Gauss; microwave power 0.5 mW; sweep width 100 mT; number of points 2500; spectrum is average of 30 scans, temperature 6.5 K (see supplementary material S1 of this paper for parameters used for simulation).

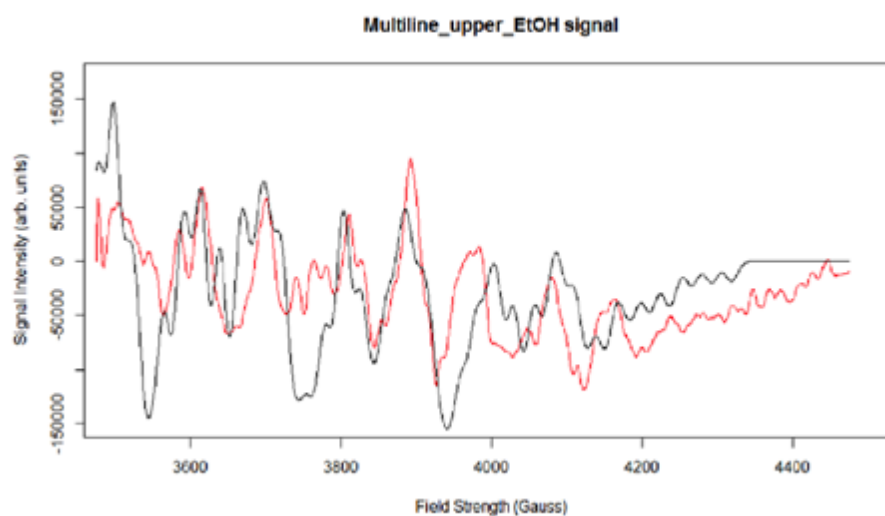


Figure 1b: The X-band CW-EPR difference up- field ML region. Experimental spectrum (red) and best-fit simulation (black). Spectrometer conditions: centre field 397.5 mT; frequency 9.634261 GHz; modulation amplitude 9.6 Gauss; microwave power 0.5 mW; sweep width 100 mT; number of points 2500; spectrum is average of 30 scans; temperature 6.5 K (see supplementary material S2 of this paper for parameters used for simulation).

near 'isolated' Mn (III-IV) dimer scheme, while the smaller coupling approximately described the 'super-hyperfine' substructure seen within the main multiline (ML) pattern lines. The presence of at least two strongly anisotropic couplings implies the presence of at least two Mn^{III} ions, i.e., the low oxidation state paradigm. The CW simulations performed by [5] gave reasonable, semi-quantitative fits to the spectra, but were clearly somewhat deficient (too well defined substructure detail), particularly near the ML pattern edges. Since there were earlier indications from the NIR turnover experiments that the ML centre was probably not homogeneous, particularly with respect to factors affecting this fine substructure, it was decided to examine this issue

further, using the 3% ethanol sample system that is known to produce the most structured forms of the broad ML species. The possibility of a statistical spread of the smaller, anisotropic coupling values being present in samples as conventionally prepared was tested. Using the excellent X-band CW-EPR generated S₂ multiline signals that were generated from high quality spinach PSII membranes preparations, with 3% EtOH in the buffer, as prepared in this project, the current proposal by [5] was tested to see if indeed Mn1 and Mn2 contribute the largest hyperfine values, with a variable anisotropic contribution from one other ion. A procedure of weighted computations was used, in an attempt to enhance the overall precision of simulations as well

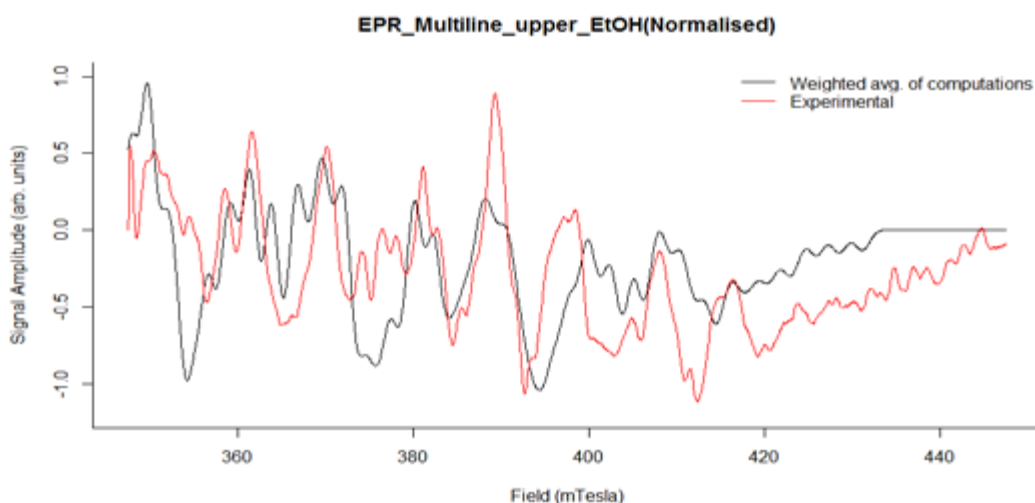


Figure 2: The X-band CW-EPR difference up-field ML region. Experimental spectrum (red) and best-fit simulation (black), which was the average of 3 weighted computations. Spectrometer conditions: centre field 397.5 mT; frequency 9.634261 GHz; modulation amplitude 9.6 Gauss; microwave power 0.5 mW; sweep width 100 mT; number of points 2500; spectrum is average of 30 scans; temperature 6.5 K. The parameters used for simulations are listed in table 1, as well as weighted average of computations method in supplementary material S3 of this paper.

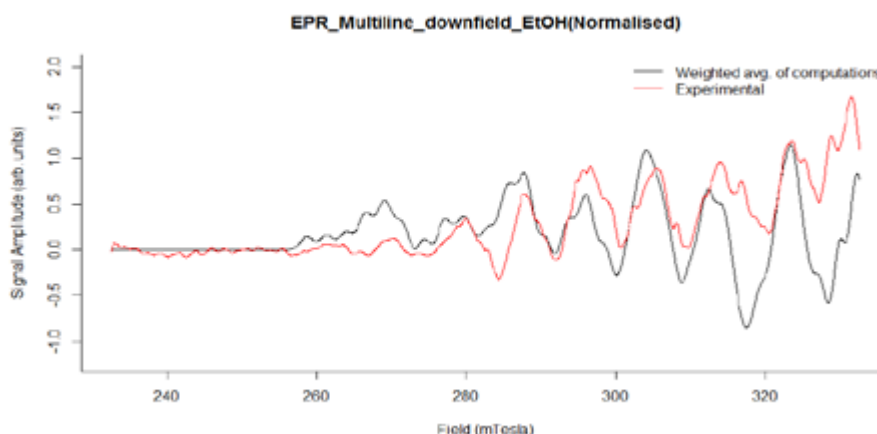


Figure 3: The X-band CW-EPR difference down-field ML region. Experimental spectrum (red) and best-fit simulation (black), which was the average of 3 weighted computations. Spectrometer conditions: centre field 282.5 mT; frequency 9.634273 GHz; modulation amplitude 9.6 Gauss; microwave power 0.5 mW; sweep width 100 mT; number of points 2500; spectrum is average of 30 scans, temperature 6.5 K. The parameters used for simulations are listed in table 1, as well as weighted average of computations method in supplementary material s4 of this paper.

as to more realistically simulate peaks at the edges, the pattern and the line sub-structure observed, particularly in the up-field region of MLS.

Materials and Methods

PSII Sample Preparations

The protocol used in isolating the fresh market English spinach (*Spinacia oleracea*), PSII containing thylakoids membranes was based on [6] with modifications by [7]. The homogenization, incubation steps as well as centrifugation were carried out in dim-green-light cold room, with temperature of about 4°C. The chlorophyll concentration determination was determined by using the method by [8]. Aliquots of 5-10 ml were placed in falcon tubes and stored at 8 to 15 mg/ml chlorophyll at -80°C in the storage buffer (pH 6) consisting of 400 mM

sucrose, 15 mM NaCl, 10 mM MgCl₂, 20 mM MES, 5 mM CaCl₂ for later use. For this experiment samples were prepared with 3% (v/v) ethanol (EtOH).

Illumination

The PSII samples (~3% EtOH), prepared as described above, were thawed on ice/water mix (0°C/273K) for 1 hour before use. Aliquots of 250 μ l were carefully loaded into 4 mm O.D. quartz EPR tubes (Wilmad quartz), and subsequently frozen in liquid nitrogen. If bubbles were found in the sample, it was immediately thawed, the bubbles removed then re-frozen in liquid nitrogen (about 77 K). The annealing of PSII sample was done by storing the sample in ice/water mix (0°C/273K) covered with a black cloth to minimise stray light entering. The sample was annealed for approximately 10 to 30 minutes,

this ensured a full relaxation to the S_1 state, and subsequently freeze trapped in the S_1 state using liquid nitrogen. The S_1 state generates the background EPR spectrum, which is subtracted from an illumination spectrum to achieve the difference spectrum. The tyrosine radical (Y_D) signal was also removed from the difference spectrum. Otherwise the remaining tyrosine radical signal was subtracted using the Bruker WIN EPR system software package. In order to generate the S_2 state signal, samples were subjected to continuous illumination at specific temperatures and wavelength ranges of light. To generate the S_2 state through $S_1 \rightarrow S_2$ turnover, from PSII membranes, the temperature of the sample was monitored and controlled by a nitrogen gas flow system. Samples were subjected to 2 minutes illumination (temperature ~200 K) using a Kodak Ektalite 1500 slide projector fitted with Halogen lamp (250 W). The light was passed through a 10 cm water path IR filter (to influence the S_1 to S_2 turnover, see [7]), filtered using a combination of yellow and blue filters to allow a narrow window green light to pass. The sample was rapidly freeze trapped in the S_2 state immediately after illumination in liquid nitrogen (77 K).

EPR Measurements

The experiments were performed using the X-band continuous wave (CW) Bruker Biospin ELEXSYS E500 spectrometer using Bruker SHQX resonant cavity and super X-EPR Microwave Bridge. The spectrometer was fitted with Oxford - ES900 continuous flow helium cryostat with temperatures controlled using Oxford Instruments ITC-4 temperature controller. The experiments were carried out at cryogenic temperatures (~6.5K). The EPR parameters used are listed in the Figure legends; the magnetic field was calibrated with Bruker ER035M NMR Gaussmeter.

Results and Discussion

^{55}Mn hyperfine interactions above 400 MHz, ranging from ~50 to ~680 MHz as seen in the S_2 multiline signal in plant PSII core complexes [5]. The 'pure' broad ML form generated from the PSII membrane samples, in the presence of ethanol (~3% EtOH), used in this part of the present project, exhibited the highly structured multiline spectra, similar to the that observed earlier by [5] in PSII core complex ML spectra (see Figures 1-7). Figures 1a and 1b shows the simulation of the experimental ML spectrum, using values close to the original hyperfine

parameter set of Ref. [5] (Table 1). As noted in the methods, this CW simulation is approximate, neglecting nuclear quadrupole terms (particularly on Mn1, where this is significant). However, full matrix diagonalization was prohibitively expensive, computationally, for this four centre system. Although there is quite a reasonable match of the simulation to the data over much of the spectrum, near the edges the match is poorer, with too much 'regular' detail from the small hyperfine parameters (Mn3 particularly) present in the simulation. Examination of the simple splitting diagram shows that small variations in the two large couplings (Mn1 in particular) will vary the resultant hyperfine line positions mostly at the edges (where the nuclear m_I values are $\pm 5/2$). Thus a (small) variation-spread in the Mn1 and Mn2 parameter magnitudes will 'blur' (through overlapping interference) fine features (from Mn3 and 4) most at the ML pattern edges. This is the basis of the approach taken here. Obviously there is a lot of potential 'freedom' in choosing such a parameter spread, which still must be relatively small, otherwise all fine detail in the ML pattern would be lost. Several possibilities were examined and the two most promising are indicated here. The weighted computation method used depends on varying both the precise hyperfine values and their statistical weights (fractional contributions to the total spectrum). The mean values about which this spread occurs are taken essentially as those determined earlier by Ref. [5] (i.e., Table 1 values). Only variations in the Mn1 and 2 hyperfine parameters were considered, with variation magnitudes of order ~5 MHz. In the first case, an average of three weighted contributions (Figures 2-4) was employed in simulating the X-band CW-EPR spectra; where simulation data 'a' was multiplied by 0.5, simulation data 'b' by 1 and simulation data 'c' was again multiplied by 0.5 (weights 0.5, 1, 0.5 respectively). In simulation 'a', 5 MHz was subtracted from each of the Mn1 (A_{Mn1x} , A_{Mn1y} and A_{Mn1z}) and Mn2 (A_{Mn2x} , A_{Mn2y} and A_{Mn2z}) hyperfine values (from Table 1) and in simulation 'c', 5 MHz was added, while simulation 'b' retained the unaltered (mean) values. The second example involved an average of seven weighted computations (Figures 5-7) in simulating the X-band CW-EPR spectra, where simulation data 'a2' was multiplied by 0.2, data 'b2' by 0.5, data 'c2' by 0.7 (NB. Simulation data 'a2', 'c2' and 'b2' representation was used to distinguish from the average of three weighted computations above), data 'd' by 1, data 'e' by 0.7, data 'f' by 0.5 and simulation data 'g' was multiplied by 0.2 (weights 0.2, 0.5, 0.7, 1, 0.7, 0.5, 0.2 respectively). The simulation data set 'a2' involved subtracting 5 MHz from each of the Mn1 (A_{Mn1x} ,

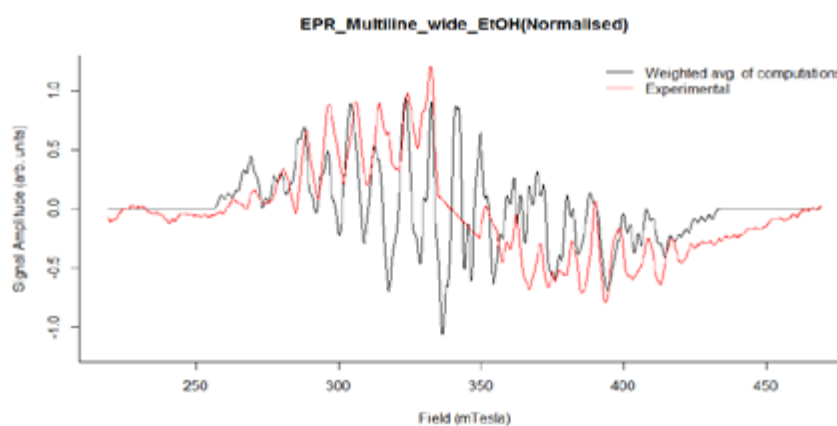


Figure 4: The X-band CW-EPR difference multiline wide experimental spectrum (red) and best-fit simulation (black), which was the average of 3 weighted computations. Spectrometer conditions: centre field 344 mT; frequency 9.634187 GHz; modulation amplitude 9.6 Gauss; microwave power 1 mW; sweep width 250 mT; number of points 2500; spectrum is average of 30 scans; temperature 6.5 K. The parameters used for simulations are listed in Table 1, as well as weighted average of computations method in supplementary material S5 of this paper.

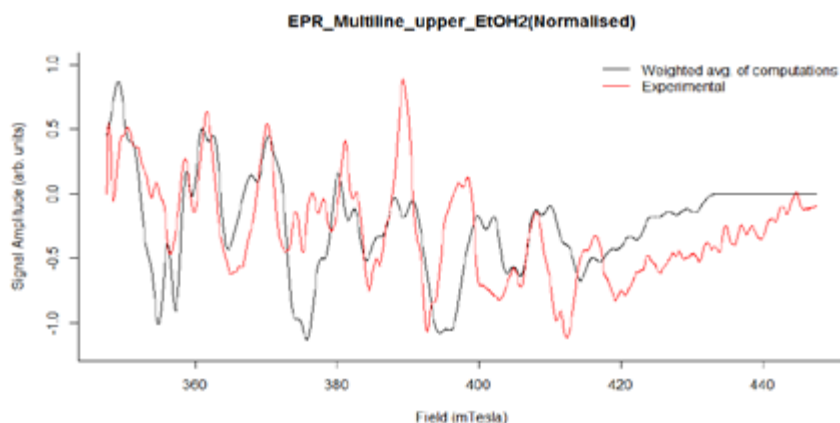


Figure 5: The X-band CW-EPR difference up- field ML region. Experimental spectrum (red) and best-fit simulation (black), which was the average of 7 weighted computations. Spectrometer conditions: centre field 397.5 mT; frequency 9.634261 GHz; modulation amplitude 9.6 Gauss; microwave power 0.5 mW; sweep width 100 mT; number of points 2500; spectrum is average of 30 scans; temperature 6.5 K. The parameters used for simulations are listed in table 1, as well as weighted average of computations method in supplementary material S6 of this paper.

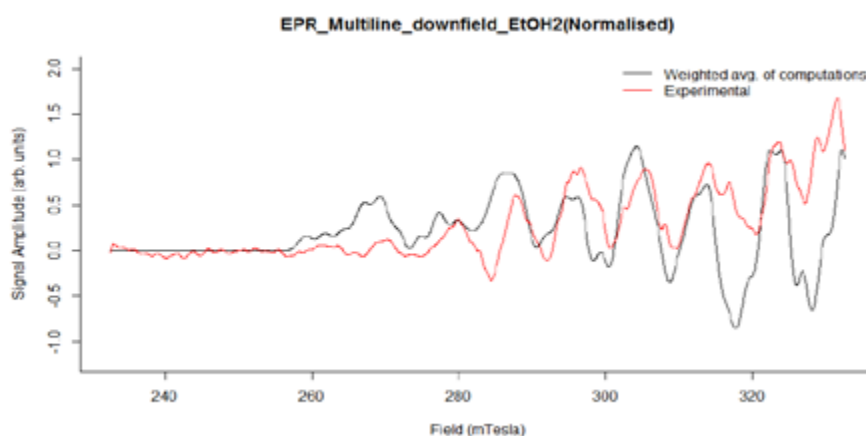


Figure 6: The X-band CW-EPR difference down- field ML region. Experimental spectrum (red) and best-fit simulation (black), which was the average of 7 weighted computations. Spectrometer conditions: centre field 282.5 mT; frequency 9.634273 GHz; modulation amplitude 9.6 Gauss; microwave power 0.5 mW; sweep width 100 mT; number of points 2500; spectrum is average of 30 scans; temperature 6.5 K. The parameters used for simulations are listed in table 1, as well as weighted average of computations method in supplementary material S7 of this paper.

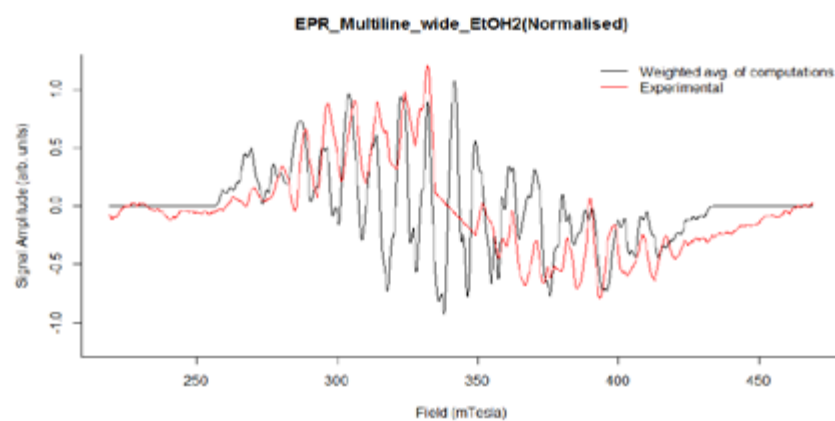


Figure 7: The X-band CW-EPR difference multiline wide experimental spectrum (red) and best-fit simulation (black), which was the average of 7 weighted computations.

Parameter	x	y	z	Isotropic value
g	1.989	2.008	1.964	1.987
A_{Mn1}	-600	-542	-320	-487
A_{Mn2}	165	237	276	226
A_{Mn3}	-78	-12	-46	-45
A_{Mn4}	1	20	1	7
Euler angles	α	β	γ	-
Mn1	0	0	0	-
Mn2	0.422	0.750	-0.737	-
Mn3	-0.136	0.210	0.378	-
Mn4	0	0	0	-
Linewidth	16 Gauss			

Table 1: Showing fitted simulation (2nd order perturbation theory) parameters to the X-band CW-EPR S₂ multiline signal (broad, down-field and upper field) of the PSII membrane plus ~3% EtOH samples. The isotropic values were calculated from $A_{Mn,i,iso} = (A_{Mn,i,x} + A_{Mn,i,y} + A_{Mn,i,z})/3$, where $i=1-4$, and $g_{iso} = (g_x + g_y + g_z)/3$. Units for A-values are in MHz, Euler angles in radians, $\nu \sim 9.634187$ GHz, line-width 1.6 mT. (NB. The hyperfine values indicated were taken as 'the central mean' in performing the weighted computations method).

A_{Mn1} and A_{Mn2}) and Mn2 (A_{Mn1x}, A_{Mn1y} and A_{Mn1z}) central hyperfine values, data 'b2' by subtracting 4 MHz from the central values, data 'c2' by subtracting 2 MHz from the central values, while data set 'd' retained the central values. Simulation data sets e, f, and g involved respective addition of the above increments to the central values (increment values -5, -4, -2, 0, +2, +4, +5 MHz respectively). The simulations of the X-band CW-EPR generated S₂ multiline signals were performed in Easy spin function 'pepper' [9] using the 2nd perturbation option (4 manganese ions). As noted the nuclear quadrupole interactions were not included. The initial estimates of the hyperfine tensors and g tensors were obtained from [5] with some adjustments in the Mn1 and Mn2 hyperfine values, line-width 1.6 mT as well as Mn3 Euler angles (α and γ). The simulated spectra are shown in Figures 2-7, and the central parameters used are listed in Table 1 below. The computer simulation of the multiline signal yielded the black spectra (after averaging three weighted computations, see Figures 2-4, and seven weighted computations, see Figures 5-7). The experimental spectra are represented in red in these figures. Spectrometer conditions: centre field 344 mT; frequency 9.634187 GHz; modulation amplitude 9.6 Gauss; microwave power 1 mW; sweep width 250 mT; number of points 2500; spectrum is average of 30 scans; temperature 6.5 K. The parameters used for simulations are listed in Table 1, as well as weighted average of computations method in supplementary material S8 of this paper. As concluded by [5] the A_{IV} term from Mn2 is reasonably isotropic and determines the ~ 90 Gauss main line pattern spacing in anti-ferromagnetically coupled Mn^{III}-Mn^{IV} dimers [10,11]. The ML region near g=2 exhibits some deviation from the simulated values [5], which reflects imperfect subtraction of the strong background features (mainly Y_D) in the difference spectrum. Figures 3 and 6 represent the expanded downfield (below g=2) region of the 'pure broad' multiline wide spectrum generated, with less evidence of pattern splitting compared to the up- field (above g=2) region of the spectrum, in Figures 2 and 5. This means, that it likely arises not from an intrinsic line-width effect, but from an anisotropic hyperfine interaction [5]. This is further supported by the fact that the splitting is not uniform on each main line of the pattern, but seen approximately on every second resonance in the upper field region, with a coupling of ~30 Gauss. Most likely this arises from Mn3, which like Mn1, is highly anisotropic in symmetry, although the overall magnitude of its contribution is small. Hence one centre should have a small ρ value as [5] earlier suggested (~0.2, which is consistent with Mn3 from Table 1, where 45/226 ~ 0.2), that the OEC cluster should have two centres with small ρ -values, was

also predicted by density matrix renormalisation group theory, which is the highest -level quantum chemical calculation yet performed on the OEC [12]. These calculations also predicted one large ρ value (~ 2) and one intermediate coupling ($\rho \sim -1$), even though a high oxidation state assumption was used for the OEC. The large coupling was for the single Mn III centre, which was Mn1 [12]. The parameters used here in simulating the multiline signal, as indicated in Table 1, also show large nuclear hyperfine values for Mn1 and Mn2, consistent with ρ values of ~2 and -1, respectively, while nuclear hyperfine values for Mn3 and Mn4 are less than 100 MHz, consistent with the results of [5]. Quadrupole interactions were not included in these simulations, but the nuclear hyperfine values for Mn4 are very small and from Table 1, the hyperfine values for Mn1 and Mn3 are highly anisotropic and almost rhombic, which means they must have Mn^{III} oxidation states, as [5] proposed. Mn2 hyperfine values are the least anisotropic, so the likely oxidation state of this ion is Mn^{IV}. The fitted parameters for Mn4 are very small but also highly anisotropic, hence this ion is likely to be Mn^{III}. The isotropic values (A_{iso}) of Mn1 and Mn2 are -487 and 226 respectively, which is consistent with the above suggested spin projection values. The maximum hyperfine coupling for Mn1 is ~600 MHz (A_{Mn1x}), with a total anisotropic range of ~280 MHz. The Mn1 hyperfine tensor has a high degree of anisotropy (280/487*100) ~57%, making it near rhombic (matching the conclusion of [5]. Mn2 has a maximum hyperfine tensor coupling of ~276 MHz, with a total anisotropic range of 111, giving a fractional anisotropy of (111/226*100) ~49%, which is substantial anisotropy for a Mn^{IV} centre. Mn3 has maximum hyperfine tensor coupling of ~78 MHz, and A_{iso} of ~45, with a hyperfine tensor, which is completely anisotropic (rhombic). Again Mn4 has A_{iso} of ~7 and is also totally rhombic in symmetry. Therefore based on this simulation, the likely oxidation paradigm of the manganese cluster is Mn^{III} Mn^{IV} Mn^{III} Mn^{III}, the 'low' oxidation state paradigm. The large magnetic exchange coupling contributions come from Mn1 and Mn2, while Mn3 and Mn4 contributions are small <100 MHz. This is totally consistent with the 'dimer of dimers'. Lastly, the results in Figures 2-7 support the idea that some statistical spread in Mn hyperfine parameter values, particularly for Mn1 and Mn2, are present in the S₂ state as conventionally prepared, even the highly resolved broad form examined here. The cosmetic fits, particularly near the pattern edges are improved with this assumption, although it is clear that the precise nature of this parameter spread is yet to be fully understood. Interestingly, the three-component weighted average spectra in Figures 2-4 is probably a better fit to the data than the seven component weighted average spectra, suggesting that perhaps only a small number of near-equivalent-ML forms are co-generated in the experimental spectra. Presumably only some of these are then responsive to NIR induced turnover to the g4.1 state of S₂.

Conclusion

The multiline signal simulation, favour the oxidation pattern of the manganese cluster to be Mn^{III} Mn^{IV} Mn^{III} Mn^{III}, which is referred to as the 'low' oxidation state paradigm in the S₂ state. The simulations of the X-band CW-EPR multiline spectra, revealed the presence of three manganese ions having hyperfine couplings with large anisotropy, which makes them likely to be Mn^{III}. This clearly support the 'low' oxidation state paradigm model, with the mean oxidation level of 3.25 in the S₂ state. This agrees with the earlier data of [5]. However, the simulations suggest that there is likely a degree of heterogeneity in the Mn hyperfine couplings, probably of Mn1 and Mn2, in the S₂ ML state, as conventionally prepared.

Author Contributions

Dr Bernard Baituti-prepared the PSII samples and performed EPR measurements, performed the simulations, prepared the manuscript (baitutib@biust.ac.bw).

Acknowledgements

The author gratefully acknowledges financial support from the Australian Research Council. Bernard Baituti also acknowledges the generous scholarships provided by the Botswana International University of Science and Technology (BIUST) and ANU.

References

1. Dismukes GC, Siderer Y (1981) Intermediates of a polynuclear manganese center involved in photosynthetic oxidation of water. *Proceedings of the National Academy of Sciences of the United States of America* 78: 274-278.
2. Gatt P, Stranger R, Pace R (2011) Application of computational chemistry to understanding the structure and mechanism of the Mn catalytic site in photosystem II - A Review. *JPPB* 104: 80-93.
3. Ahrling K, Pace R, Evans M (2005) The Catalytic Manganese Cluster: Implications from Spectroscopy. In: Thomas J, Kimiyuki S (ed.), *Photosystem II the Light Driven Water: Plastoquinone Oxidoreductase*, Springer, The Netherlands, pp: 285-305.
4. Blondin G (1997) Electron paramagnetic resonance study of the S=1/2 ground state of a radiolysis-generated manganese(III)-trimanganese(IV) form of [Mn-IV;O-4(6)(bipy)(6)](4+) (bipy=2,2'-bipyridine). Comparison with the photosynthetic Oxygen Evolving Complex. *J Chem Soc-Dalt Trans* 21: 4069-4074.
5. Jin L (2014) Electronic structure of the oxygen evolving complex in photosystem II, as revealed by (55)Mn Davies ENDOR studies at 2.5 K. *PCCP* 16: 7799-812.
6. Bricker TM, Pakrasi HB, Sherman LA (1985) Characterization of a spinach photosystem II core preparation isolated by a simplified method. *ABB* 237: 170-176.
7. Smith PJ, Ahrling KA, Pace RJ (1993) Nature of the S₂ state electron paramagnetic resonance signals from the oxygen-evolving complex of photosystem II: Q-band and oriented X-band studies. *J of Chem Soci* 89: 2863-2868.
8. Porra RJ, Thompson WA, Kriedemann PE (1989) *Biochimica et Biophysica Acta* 975: 384-394.
9. Stoll S, Schweiger A (2006) EasySpin, a comprehensive software package for spectral simulation and analysis in EPR. *J of Magne Reson* 178: 42-55.
10. Teutloff C (2005) High-field EPR investigations of Mn_{III}Mn_{IV} and Mn_{II}Mn_{III} states of dimanganese catalase and related model systems. *Magne Resona in Chemis* 43.
11. Schäfer KO (2003) Multifrequency EPR investigation of dimanganese catalase and related Mn(III)Mn(IV) complexes. *J of Phys Chem B* 107: 1242-1250.
12. Kurashige Y, Chan GKL, Yanai T (2013) Entangled quantum electronic wavefunctions of the Mn-CaO-cluster in photosystem II. *Nature Chemistry* 5: 660-666.